View Article Online / Journal Homepage / Table of Contents for this issue

A model of non-congruent laser ablation as a source of fractionation effects in LA-ICP-MS

Roland Hergenröder

Received 18th January 2006, Accepted 24th March 2006
First published as an Advance Article on the web 11th April 2006
DOI: 10.1039/b600698a

Published on 11 April 2006. Downloaded by Michigan State University on 19/01/2016 15:49:27.

A model for laser ablation under conditions which are typical for LA-ICP-MS (He or Ar atmosphere, fluences below 100 J cm^{-2}) is proposed that identifies the melted and subsequently re-solidified portion of the heated sample as a possible source for element-specific fractionation. Based on the full 3-dimensional description of the heat conduction problem, the heating, melting and evaporation of a sample is analytically modelled. Incorporation of radial heat losses provides a more realistic picture of the achievable surface temperature. Owing to the division of the ablation zone into a congruently vaporized part with stoichiometric mass removal and a zone of non-stoichiometric evaporation, the portion that laser ablation contributes to the total fractionation in LA-ICP-MS can be identified. The model describes the fluence dependence of fractionation, explains the size-dependent chemical composition of the particles, and the influence of the atmosphere on laser sampling. The theoretical predictions are compared with literature data and a fairly good agreement is found, especially for dilute alloys. Based on the model, optimal conditions for laser sampling in relation to a specific sample can be identified.

1. Introduction

Laser ablation ICP-MS is one of the most suitable techniques for direct solid analysis. Laser ablation does not require a complicated sample preparation procedure, so the risk of contamination or sample loss can be avoided. Furthermore, laser mass spectrometry is capable of providing topo-chemical information with high spatial resolution and sensitivity. The benefits of the highly intense, monochromatic, coherent, and directional radiation of lasers have been exploited and successfully used in mass spectrometric experiments and applications which are well documented in several reviews.[1–4]

However, there are problems that remain in all laser ablation based methods. At best, laser ablation based methods such as LIMS or LIBS can be called semi-quantitative analytical methods. Even a technique like LA-ICP-MS, which is a very sensitive and powerful method, is constantly hindered by matrix effects, elemental fractionation and non-linear calibration graphs, which are related to the ablation process, the aerosol transport, and the vaporization, atomization and ionization of the laser generated aerosol.[5] There are strategies around these problems. However, they have to be solved case by case.[6–8] A deeper understanding of the laser sampling process reveals that, at least partly, these inherent problems are caused by inappropriate laser sampling conditions or by the hyphenation of laser ablation with ICP-MS instruments that are basically not built or optimised for this coalition at present.

The problem of mass removal under the effects of laser radiation encompasses a wide range of issues which, somewhat arbitrarily, can be divided in the internal and external problem.[9,10] The internal problem deals with the processes occurring in the condensed material: heating and movement of interfaces, melting, and evaporation, whereas the external problem covers issues such as the motion of vapour, plasma formation, hydrodynamic sputtering, and particle condensation. Hydrodynamic sputtering describes a class of possible mechanical liquid–plasma interactions which can act as a source for the coarse particle component in laser generated aerosols.[11,12] It is the internal problem that will be discussed in this article. It covers direct laser–sample interaction and tries to identify possible sources for deficient laser sampling with regard to the potential of the detection system—for example, the generation of particles too large to be evaporated by an ICP. Clearly, an aerosol containing particles of sizes that are not evaporated can add new obstacles to a correct analysis.

The developing plasma influences the internal processes to a certain extent.[13,14] Plasma-shielding can diminish the laser radiation that can reach the sample surface. Owing to the recoil pressure of the plasma a melt layer in the sample zone can be thrust aside, resulting in the pile up of material around the laser crater and the ejection of extra material in the form of large particles.[15] The interrelation between internal and external problems will be the topic of a future article and are only briefly discussed here where necessary.

There is a long lasting discussion concerning which laser and laser parameter or other conditions are beneficial for laser sampling. From the beginning of LA-ICP-MS key parameters such as laser wavelength and energy, beam profile, or background gas, have been identified as such and investigated.[6] Often the results have been controversial and not conclusive. Clearly, one of the main reasons for this situation is the strong mutual dependence between different parameters and the difficulty in separating coupled phenomena without a clear

ISAS—Institute for Analytical Sciences, Bunsen-Kirchhoff Str. 11, 44139 Dortmund, Germany

View Article Online

Published on 11 April 2006. Downloaded by Michigan State University on 19/01/2016 15:49:27.

picture of the overall process. A second reason is the fact that the analytical characteristics are not always directly linked to physical parameters, *e.g.*, a change in laser wavelength results not only in a different sample absorption and reflection, but is also related to a change in plasma absorption, sometimes to a change in the size distribution of particles which influences the ICP performance (*e.g.*, fractionation due to incomplete evaporation, atomization and ionization of large particles or elemental bias due to overload of the plasma), which collectively combine to cause a change in precision, accuracy and achievable detection limit. One of the goals of this article is to outline the relationship between different parameters and to distinguish the underlying effects. The separation of effects, and where possible the outline of criteria that allow us to judge how reliable a partitioning of phenomena is, should improve the situation.

The term "congruent/non-congruent vaporization", which is common in laser material processing, is used to distinguish the possible element biasing during the laser ablation event from other fractionation effects (*e.g.*, transport, evaporation in the ICP) that can occur. The terms "vaporization" and "evaporation" are used to distinguish between kinetically controlled mass removal and removal under thermodynamic equilibrium condition maintained by diffusion, respectively. The conditions for the appearance of different modes of thermal mass removal are the subject of the following model.

2. Description of the model

Single pulse laser–material interaction lays the foundation for all subsequent processes, sometimes even including the interaction of the next laser pulse with the sample.[16] Therefore, adequate description and understanding of single pulse interaction is mandatory.

The interaction mechanisms between laser light and matter depend on the parameters of the laser beam and the physical and chemical properties of the material. Laser parameters are the wavelength, intensity, spatial and temporal coherence, polarization, angle of incidence, pulse duration, and repetition rate. The material is characterized by its chemical composition, microstructure, homogeneity and the locally related physical characteristics like absorption coefficient, melting and vaporization enthalpy. An understanding and solution of the problems in laser sampling requires a link between these two sets of parameters. It is clear that a single theory to describe all possible processes is not at hand and would be far too complex for practical purposes. As an alternative, numerical models can be set up.[17] They will be a useful tool in the future. However, it will still be necessary to decide what processes have to be included.

The special use of lasers for analytical purposes places some constraints on the experimental situation, which makes the problem, to a certain degree, treatable. Research in the last couple of years has provided a vast amount of results which converge to certain laser types and parameters that have been proved to yield the best results. Clearly, practical considerations are always part of the choice for a specific laser type. However, as will be shown, there are also very clear physical reasons for the trends. Based on this well-established praxis specific parameter sets are common for analytical applications. According to these parameters only certain laser types, which are listed in Table 1, have found their way into the laboratory and these will be the basis for the following considerations. The wavelengths that will be specifically considered are centred on 0.2 μm and 1.0 μm. Shorter wavelengths are increasingly impractical due to particular optical requirements, purged beam paths, and complicated laser systems (*e.g.*, F_2 laser). In addition, real advantages are questionable, as will be discussed later.

Table 1 Commonly used laser types in LA-ICP-MS and related sample techniques

Laser	Wavelength (λ)/nm	Energy/eV	Pulse length (τ_L)
Nd:YAG	213	5.82	~10 ns
	266	4.66	~10 ns
	1064	1.17	~10 ns
Ti:sapphire	780	1.59	~100 fs
	266	4.66	~100 fs
ArF	193	6.42	10–20 ns
KrF	248	5.0	10–20 ns
XeCl	308	4.03	10–20 ns

At the IR side of the spectrum, 1 μm is regarded as a boundary because, besides practical considerations, longer wavelengths show basically the same absorption mechanism but with lower efficiency than a Nd:YAG laser centred at 1 μm in most materials. Only in the far-IR are new aspects likely to occur due to direct excitation of the ionic and molecular parts of the material. Additionally, it has been shown that short (~1 ns) and ultra-short (<1 ps) are advantageous. Far-IR lasers with these characteristics are currently not available. Wavelengths in between these two regimes do not offer really new aspects, if no specific absorption is met.[18]

Next to the wavelength aspect, the influence of laser energy, fluence, or intensity has been evaluated. Depending on the material, a working regime between 1–10 mJ, which translates into fluences between 1–100 J cm^{-2} or intensities between 10^8–10^{13} W cm^{-2}, has been found beneficial for most applications.[4,19–23] The regime above 10^{10} W cm^{-2} is only reached with ultra-short (<1 ps) laser pulses.

As has already been mentioned, currently only lasers with pulse durations around 10 ns are in use. Longer pulses are unambiguously less useful, as will be seen later. This has been demonstrated not only for analytical applications but also for conceptually similar applications like pulsed laser deposition, laser machining, or medical applications.[24] Laser pulses in the picosecond range have also been studied. However, they have not been proved superior compared with ns pulses.[25,26] Recently, laser systems with pulse lengths around 100 fs have become available and have been studied for analytical purposes.[27–30] They do add totally new aspects to the ablation process which can be understood against the background of the concept outlined in the following.

2.1. The three-dimensional heat equation

Under the conditions described the ablation process can be regarded as thermal. It is only in very special applications (*e.g.*,

 This journal is © The Royal Society of Chemistry 2006

View Article Online

Published on 11 April 2006. Downloaded by Michigan State University on 19/01/2016 15:49:27.

polymers and UV irradiation) non-thermal ablation—photophysical material removal—plays a role.[24,31] A proper definition of *thermal* ablation is difficult. It would require a detailed knowledge of the fundamental interactions between laser light and matter, and of the various relaxation times involved, information which is, for a typical sample, not available and a task which is far beyond the scope of this article. Therefore, a more practical, problem-oriented definition will be used. *Thermal ablation is a process which describes the material removal as an evaporation process from the condensed surface*. This definition implies that a system can proceed through non-equilibrium states during excitation, relaxation, and distribution of the absorbed energy but phase changes from liquid or solid to vapour can be described as surface evaporation of the Arrhenius type.[31] Based on the thermal ablation model, the conceptual idea behind the following theoretical treatment is as follows.

- First, the radial 3D heat equation is employed to calculate the temperature distribution in a single component sample under ablating conditions with moving interfaces.
- The temperature distribution allows determination of the partitioning between evaporated and melted/resolidified material.
- The partitioning is used as the basis of a second simplification: the evaporated volume is treated in the limiting case of strong non-equilibrium, congruent vaporization, whereas the melt pool is treated under evaporation equilibrium, as the source of non-congruent (fractionated) material evaporation.

The second simplification allows the incorporation of additional chemical components to study non-congruent evaporation. Dilute alloys (*i.e.*, material systems that can be treated as a solution with a minor alloying component) are the best model system to be compared with the results. The addition of solute to a pure metal changes in principle the melting, evaporation and crystallization processes and their kinetics. For dilute alloys this influence can be neglected. Here, the major component determines the melting and evaporation kinetics and the minor constituents are only introduced into the "heat-bath" of the melt. However, it will be shown that even for glasses the results are, at least qualitatively, usable.

Starting from this idea the radial 3-dimensional heat equation has to be solved[32]

$$\frac{\partial \Delta H_S}{\partial t} = v_{LV}\frac{\partial \Delta H_S}{\partial z} + \frac{\partial}{\partial z}\left(\kappa_S \frac{\partial T}{\partial z}\right) + \kappa_S \frac{1}{r}\left[\frac{\partial}{\partial r}\left(r\frac{\partial T}{\partial r}\right)\right] - \frac{\partial I_A}{\partial z} \quad (1)$$

together with the liquid–vapour boundary condition

$$-\kappa_S \frac{\partial T}{\partial z}|_{z=0} = -J_i \frac{\Delta H_V^i(T_S)}{N_A}$$

Here ΔH_S is defined as $\Delta H_S = \rho\, c_P\, T$. ΔH_V^i represents the vaporization enthalpy. ρ and κ_S are the density and heat conduction coefficient, respectively. I_A is the absorbed laser fluence. Table 2 lists the material parameters that are used throughout the calculations. The velocity ν_{LV} describes the movement of the liquid–vapour interface due to evaporation with a particle (atom) flux J_i and a total energy flux $J_i \Delta H_V^i / N_A$ from the surface. This process, which includes "sublimation" and "evaporation", describes the passage from a condensed phase (solid or liquid) to vapour by virtue of the emission of particles (atoms or molecules) from the extreme outer surface. According to the kinetic theory of gases, when a material evaporates into a gaseous medium with a partial pressure P_i of the evaporating component far away from the surface, the resultant evaporation rate near the interface is approximated by the Hertz–Langmuir–Knudsen equation.[33,34]

$$J_i = J_+ - J_- = \frac{\alpha_0}{(2\pi(M_i/N_A)k_B T_S)^{1/2}}(P_S(T_S) - P_i) \quad (2)$$

J_+ is the flow of particles from the evaporating surface, J_- is the reverse flow of particles, P_S the saturated vapour pressure, T_S, (M_i/N_A) and α_0 are the temperature of the evaporating surface, the atomic mass, and the accommodation coefficient, respectively. The accommodation coefficient ($\alpha_0 \leq 1$) is an empirical factor which depends on the particular mechanism of evaporation. It is often denoted as the evaporation or sticking coefficient. Here, it is assumed to be $\alpha_0 = 1$. Taking the Clausius–Clapeyron relation into account and multiplying the flux J by m_i/ρ yields the maximum speed of the evaporation front.

$$v_{LV}^i = \frac{M_i}{N_A \rho_i} J_i = \left(\frac{(M_i/N_A)}{2\pi k_B T_S}\right)^{1/2} \frac{P_S(T_S)}{\rho_i} = v_0 \exp\left[-\frac{M_i \Delta H_V^i}{N_A k_B T_S}\right] \quad (3)$$

Here, ν_0 is of the order of the velocity of sound in the solid, ρ_i the density of the liquid, M_i the molecular weight, and H_V^i the vaporization enthalpy of element i, respectively. Different evaporation theories achieve basically the same (over-) exponential dependence.[9,35]

Table 2 Material parameters employed for calculation. The reflectivity R is given for two wavelengths

Material parameters	Cu	Zn	Ni	Sn	Pb	Fe
M/g mol^{-1} [a]	63.54	65.38	60.0	120	208	55.85
ρ/g cm^{-3} [a]	8.94	7.14	9.8	7.3	11.34	7.85
ΔH_V/J g^{-1} $\times$ 10^{-3} [a]	4.6	1.8	6.4	1.94	0.87	6.3
ΔH_m/J g^{-1} 10^{-3} [a]	0.2					
T_V/K[a]	1357	1200	3448	2705	2023	3300
c_p/J g^{-1} K^{-1} [a]	0.48					
D_{th}/cm^2 s^{-1} [b]	0.43					
R[0.2/1.0 μm][b]	0.23/0.91					

[a] T. Iida and R. I. Guthrie, *The physical properties of liquid metals*, Clarendon Press, Oxford, 1988. [b] D. Bäuerle, *Laser Processing and Chemistry*, Springer-Verlag, Berlin, 3rd edn., 2000.

View Article Online

Published on 11 April 2006. Downloaded by Michigan State University on 19/01/2016 15:49:27.

Obviously, with the last term in the in the 3-dimensional heat equation, the radial term,

$$\kappa_S \frac{1}{r}\left[\frac{\partial}{\partial r}\left(r\frac{\partial T}{\partial r}\right)\right] \approx -\kappa_S \frac{\Delta T(z)}{r_0^2}$$

additional losses due to radial heat conduction are added. Here, r_0 describes a typical length scale, *e.g.*, the beam radius.

Often one-dimensional laser ablation (*i.e.*, neglecting the radial term) is assumed on the basis that the laser spot is large compared with the ablation depth. Certainly, this assumption is true for most LIBS applications. However, for laser sampling under ICP-MS conditions the usefulness of the radius-to-depth criterion is not obvious. Often spots down to 10 μm diameter are used. Moreover, it turns out that part of the non-congruent ablation is related to the radial heat dissipation. Therefore, the one-dimensionality of the heat conducting problem is clearly linked to all heat dissipation mechanisms and a more precise criterion than radius-to-depth has to be formulated.

For stationary conditions, a flat-top intensity distribution over the laser beam profile, and assuming a paraboloid of revolution with a constant apex radius of curvature η for the ablation crater geometry, which moves along the z-axis with a constant velocity v, the following analytical solution to the 3-dimensional heat equation was found[36]

$$\nu_{LV} = I_A[\rho\Delta H_V + \rho c_P \Delta T_S f(\beta)]^{-1} \quad \text{(a)}$$

$$f(\beta) = -\frac{\exp(-\beta)}{\beta Ei(-\beta)}, \beta = \frac{v_{LV}\eta}{2D_{th}} \quad \text{(b)}$$

$$z(t) = \frac{\eta}{2} + I_A t[\rho\Delta H_V + \rho c_P \Delta T_S f(\beta)]^{-1} \quad \text{(c)}$$

$$r(z,t) = [\eta^2 + 2\eta I_A t[\rho\Delta H_V + \rho c_P \Delta T_S f(\beta) - 2\eta z]^{-1/2} \quad \text{(d)}$$

$$T(r,z,t) = T_0 + \frac{(T_S - T_0)Ei(-\beta w)}{Ei(-\beta)} \quad \text{(e)} \qquad (4)$$

Ei is the exponential integral function. $w = 1$ describes a paraboloid of revolution with an apex radius of curvature η. The depth of the crater is described by $z(t)$, $r(z,t)$ is the radius at a given depth. D_{th} is the thermal diffusivity related to κ_S through

$$D_{th} = \frac{\kappa_S}{\rho c_P}$$

In order to find ν_{LV} and T_S these equations have to be solved together with eqn. (3). The specific ablation geometry that was chosen here is close to realistic ablation craters such as are seen in numerous electron microscopy images. An interesting feature of the model is the coupling of growth in z- with r-direction. Even more notable is the inclusion of energy losses due to heat diffusion into the surrounding material. The inclusion of additional losses is necessary to achieve realistic surface temperatures for the specific laser parameters used in LA-ICP-MS (*cf.* Table 1). Two clear boundaries exist for the surface temperature. It must exceed melting temperature, and clearly lie below the critical temperature.[31,37] Often excessive, unrealistically high temperatures are claimed to be reached during laser heating, which seems to result from the negligence of additional heat sinks.[38] Fig. 1 gives the underlying model in diagrammatic form.

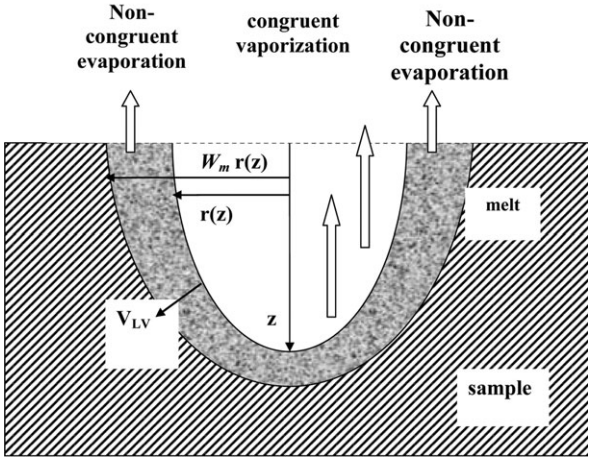

Fig. 1 The underlying model is based on the approximation that the liquid/vapour interface moves in the form of a paraboloid of revolution into the sample material. A part of the material is directly evaporated, the rest of the material within the boundaries of $T > T_{melt}$ remains in a liquid state. It is a source for non-congruent (fractionated) evaporation and hydrodynamic sputtering.

2.2. Simplified plasma absorption model

With the laser-light intensities above 10^{8-9} W cm^{-2} laser–plasma interactions like plasma shielding cannot be ignored.[10,14,25] The intensity at the ablation front depends on the layer thickness of the evaporated material which screens the ablation front:

$$I_A = I_0 (1 - R) \exp[-\alpha_g h].$$

Here, R, h, and α_g are the reflectivity, the thickness of the plasma, and the absorption coefficient of the vapour plume recalculated to the density of the condensed phase, respectively.[31,39] All optical and material parameters are assumed to be temperature independent. With the assumption of a linear mass density related to linear expansion of the plume during the laser interaction time[40] and non-specific linear absorption, the absorption coefficient α_g can be approximated by inverse Bremsstrahlung.[41]

$$I_A = I_0(1 - R)\exp\left[-1.15 \times 10^{11} \frac{t v_{LV}}{T_S^{3/2}}\right] \qquad (5)$$

The model described by eqn. (4) allows calculation of ($t\nu_{LV}$), the thickness of the evaporation layer, which is linearly expanding during the laser pulse. T_S is taken as the surface temperature for the duration of the laser pulse.

2.3. Melt solidification time

To calculate the amount of evaporated material, it is necessary to know the time until re-solidification occurs. The non-evaporated material remains liquid much longer than the laser pulse duration. Based on the Stefan model, and the assumption that convective and plasma mixing guarantees a

 This journal is © The Royal Society of Chemistry 2006

View Article Online

Published on 11 April 2006. Downloaded by Michigan State University on 19/01/2016 15:49:27.

homogenous temperature distribution in the melt, a special solution of the heat diffusion equation can be used, which yields the elapsed time until solidification is finished

$$\tau_{\mathrm{melt}} = \frac{h_{\mathrm{l}}^2}{4\xi^2 D_{\mathrm{th}}}\left(1 + \frac{4\xi\sqrt{D_{\mathrm{th}}\tau_{\mathrm{L}}}}{h_{\mathrm{l}}}\right);$$
$$p\xi(1 + \mathrm{Erf}(\xi))\exp(\xi^2) = \frac{c_{\mathrm{P}}(T_{\mathrm{melt}} - T_0)}{\sqrt{\pi}\Delta H_{\mathrm{m}}} \quad (6)$$

ξ is constant with values within $0.25 < \xi < 1$.[32] ΔH_{m}, T_0, h_{l} are melt enthalpy, the sample temperature at infinity, and the thickness of the melt layer, respectively. The melt thickness can be calculated from eqn. (4) and yields $h_{\mathrm{l}} = z(w_{\mathrm{melt}}) - z(w_{\mathrm{vapour}})$. Melt removal due to the recoil pressure is not taken into account, but it is clear that the amount of material which is pushed out of the crater should also be related to the thickness of the liquid layer. This can be seen from ablation craters at low and high fluences. Similarly, the tendency for hydrodynamic sputtering correlates with the amount of melt.[42]

The temperature far away from the laser focus drops fast to a value close to melting temperature, where it remains until the solidification front has reached the surface. During this time evaporation is low. However, depending on the amount of liquid material available fractionation can take place

3. Results and discussion

3.1. Ablation of a homogenous sample

Basically, this model allows the calculation of

- the liquid/vapour interface velocity
- the surface temperature
- the amount of evaporated material
- the ablation depth
- the thickness of the liquid layer
- the time for solidification
- laser spot size effects.

The results of the calculation are displayed in Figs. 2–6. No fitting parameter is used. Nonetheless, the calculated values are in reasonable agreement with what is considered typically under the conditions used in LA-ICP-MS. However, it is not

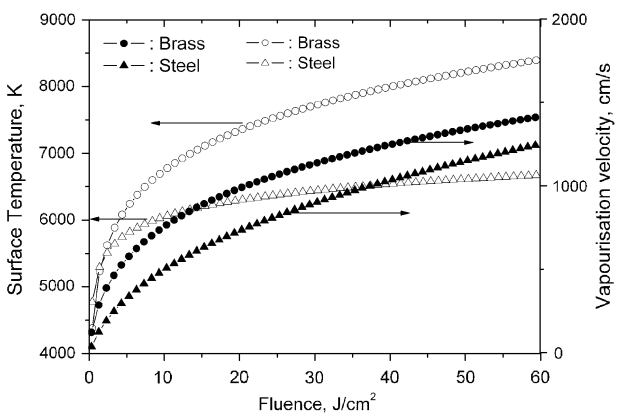

Fig. 2 Surface temperature and resulting vaporization front velocity as a function of laser fluence. The focal spot size was assumed to be 30 μm.

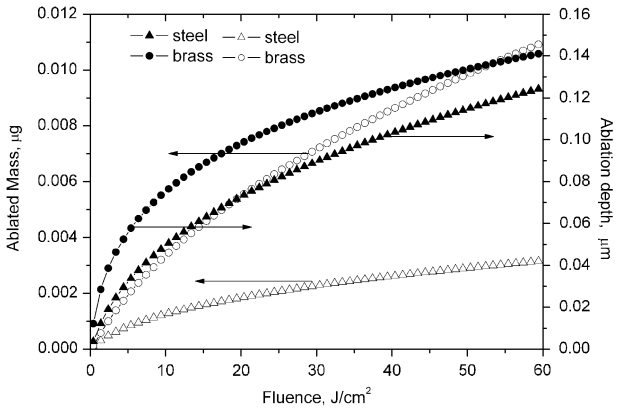

Fig. 3 Ablated mass and ablation depth as a function of laser fluence. The focal spot is assumed to be 30 μm. No melt displacement due to back pressure from the plasma is taken into account.

so much the quantitative aspect which is interesting, it is more the functional dependencies and relations given by the model which help to guide through the complexity of laser ablation. Even if the compliance with published data is good, the quantitative aspects are somehow doubtful due the difficulty in finding reliable thermodynamic data for a wide range of temperatures and realistic materials.[4,16,22,43,44]

It is interesting to compute the ratio, R_{V}, between the vaporized and the melted fraction of the heated sample as a function of β

$$R_{\mathrm{V}} = \frac{V(1)}{V(w_{\mathrm{m}})} \cong \frac{1}{w_{\mathrm{m}}(\beta)}$$

The parameter β (eqn. (4b)) can be read as the ratio between the liquid/vapour interface and the heat diffusion front velocity, v_{s} and v_{D}, respectively.

$$\beta \sim \frac{v_{\mathrm{LV}}}{v_{\mathrm{D}}} = \frac{v_{\mathrm{LV}}}{2}\sqrt{\frac{t}{D_{\mathrm{th}}}} \sim \frac{v_S l_{\mathrm{th}}}{2D_{\mathrm{th}}} \quad (7)$$

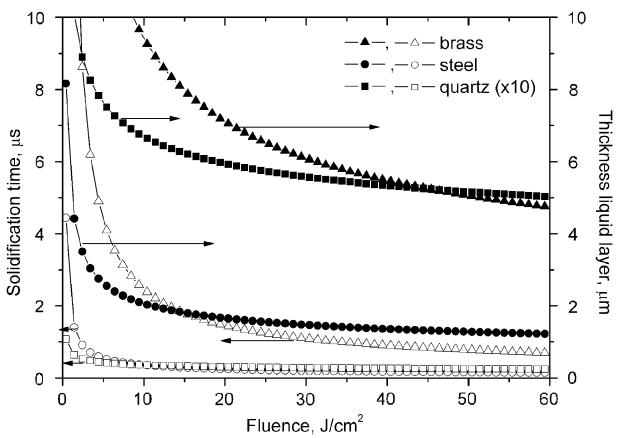

Fig. 4 Melt thickness and resulting solidification time as a function of laser fluence. With increasing absorbed laser energy the melt thickness decreases due to higher evaporation rates with the consequence that the time for solidification decreases. The shortened time in a liquid layer reduces the fractionation that can take place. A calculation for quartz is included to demonstrate the influence of a reduced heat diffusion coefficient under otherwise similar conditions.

View Article Online

Published on 11 April 2006. Downloaded by Michigan State University on 19/01/2016 15:49:27.

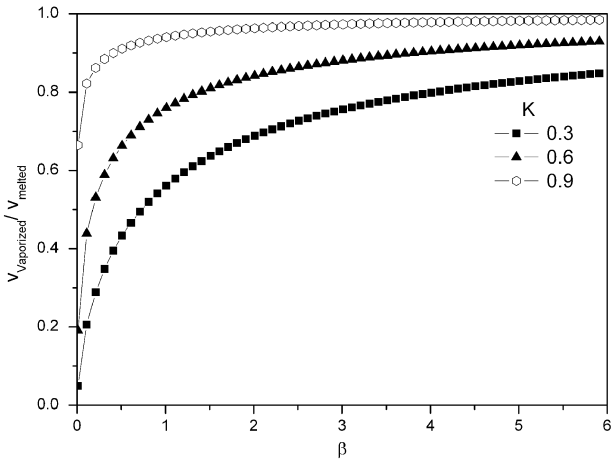

Fig. 5 The factor β is the governing factor in the transformation from 3-dimensional to 1-dimensional ablation. With an increasing β heat diffusion is less influential. *K* represents material with different melting temperature vaporized with the same surface temperature. A small *K* corresponds to a material with high melting temperature. This diagram does not allow classification of material. It only demonstrates when a 1-dimensional description is admissible.

With increasing liquid/vapour interface front velocity, v_{LS}, *i.e.*, increasing absorbed laser energy (*cf.* Fig. 2), β increases. It can be seen from Fig. 5 that with $\beta \gg 1$ the amount of evaporated relative to melted material converges slowly to a saturation level close to unity. This saturation would imply that all molten material is also evaporated. The trend is clear: high vaporization rates reduce the liquid layer, which is a source of depletion or enrichment. Additionally, the existence of a liquid layer is a necessary condition for hydrodynamic sputtering effects which must be discussed in a further article.

With the limit $\beta \gg 1$ we obtain $f(\beta) \rightarrow 1$ and eqn. (4a) develops into the solution of the 1-dimensional case.[32,36] Conditions like these allow us to neglect heat losses described by the radial term in eqn. (1). Therefore, the decision as to whether a situation can be approximated by a 1-dimensional heat equation or has to be treated as a full 3-dimensional problem has to be based on β and not only on a "large" spot size. Therefore, 1-dimensionality implies that the parasitic heat load in the surrounding material is minimized; all absorbed energy is used for the vaporization. Achieving high liquid/vapour interface velocities that comply with high surface temperatures creates a situation which is then described by a 1-dimensional model. Hence, it follows that if r_0, which can roughly be substituted by the laser spot size, is kept constant, increasing the laser radiation intensity or reducing the laser pulse duration at constant laser energy yields a larger β, which describes a situation which is closer to the analytically beneficial 1-dimensional case. The portion of the vapour phase increases, the liquid layer as a source of detrimental effects like fractionated evaporation or hydrodynamic sputtering is minimized. In addition, the achievable spatial resolution is optimized.

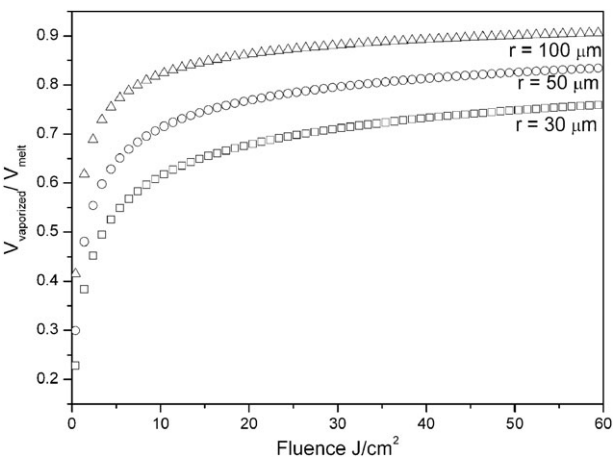

Fig. 6 The effect of laser spot size demonstrated for a brass sample. With decreasing laser focus heat diffusion due to changes in surface-to-volume ratio becomes more pronounced. With the same deposited energy a lower surface temperature is reached, resulting in decrease of the vaporized/melted material ratio.

The effect of different laser beam sizes with similar fluence has been calculated for brass and is shown in Fig. 6. The result can be read in two ways: for a given material and a given absorbed fluence, the laser diameter cannot fall below a certain value without producing excessive fractionation, or it can be interpreted as to achieve a certain spatial resolution without analytical performance penalties enough laser energy has to be delivered and absorbed by the sample. To make it clear: for a given material 5 J cm^{-2} delivered to a 50 μm spot is not the same as to a 5 μm spot. Clearly, the delivered and absorbable laser energy is limited and cannot be increased arbitrarily to improve the ablation conditions. The first limitation encountered with ns-pulses is laser plasma shielding, as has already been discussed.

Because of the high thermal diffusivity metals are a worst case scenario for laser ablation. If we consider a material such as glass, which has a 50 times lower thermal diffusivity, correspondingly higher energy confinement is achieved as the calculations in Fig. 4 demonstrate. The same figure shows that with increasing laser fluence the time for solidification decreases. This reduction is directly correlated with the diminishing melt depth due to vaporization. With increasing fluence the liquid/vapour interface velocity increases and more material is removed from the melt layer.

The next step is to make the above mentioned conceptual simplifications, which basically mean that we partition the ablation zone into melt volume and surface and evaporated volume. The melted zone will be related to the vapour pressure of the different embedded elements.

3.2. Non-congruent evaporation

Non-stoichiometric ablation is a fluence dependent effect.[19,21,22] With increasing laser fluence the ablated material matches the bulk composition asymptotically. If we assume that the non-congruent ablation is based on fractionated evaporation then the deviation from the correct composition should be proportional to the melted but not vaporized zone and the difference in the vapour pressures of the compounds. A calculation for brass confirms this idea.

 This journal is © The Royal Society of Chemistry 2006

View Article Online

Published on 11 April 2006. Downloaded by Michigan State University on 19/01/2016 15:49:27.

It is assumed that a melted zone exists around the vaporized volume (*cf*. Fig. 1). Alloying elements are evaporated from the melt zone whereas the vapour pressure of Cu is supposed to be low enough to be neglected.[45] It is assumed that no depletion zone develops into the depth of the liquid layer. This assumption is reasonable if the back pressure created by the plasma is considered, which pushes the melt out of the hole and mixes the liquid layer. Under this assumption the alloying element fraction (*e.g*. Zn) in the laser created aerosol can be written as:

$$\frac{m_{\mathrm{Zn}}}{m_{\mathrm{Cu}}+m_{\mathrm{Zn}}}=\frac{m_{\mathrm{Zn}}^{\mathrm{V}}+m_{\mathrm{Zn}}^{\mathrm{R}}}{m_{\mathrm{Cu}}^{\mathrm{V}}+m_{\mathrm{Zn}}^{\mathrm{V}}+m_{\mathrm{Zn}}^{\mathrm{R}}}$$

Here, the total mass removed from the sample is subdivided into the vaporized part, m^{V}, evaporated congruently without fractionation, and the non-congruent evaporated part from the rim of the crater, m^{R}.

The mass removed in the different partitions of the ablated zones can be approximated by

$$m_i^{\mathrm{V}} = \rho_i V$$

$$m_i^{\mathrm{R}} = \left(J_i \frac{M_i}{N_{\mathrm{A}}}\right) tF$$

With well-known formulae for objects of revolution the volume V and the area F can be calculated.

$$V(w) = \pi rw\left(\frac{rw}{2}+v_{\mathrm{LV}}t\right)^2$$

$$F(w) = \frac{4}{3}\pi\sqrt{2wr}\left((wr+v_{\mathrm{LV}}t)^{3/2}-\left(\frac{wr}{2}\right)^{3/2}\right)$$

In this model, any isothermal surface is a parabaloid of revolution parameterized by w. Therefore, the melt volume (area) is determined by solving the transcendental eqn. (4e) for $T = T_{\mathrm{melt}}$(brass). Now, it is simply assumed that during the time when the molten metal exists, $t = \tau_{\mathrm{melt}} + \tau_{\mathrm{L}} \cong \tau_{\mathrm{melt}}$, the fractional evaporation is proportional to the mass flux, $J_i(T_{\mathrm{S}})M_i/N_{\mathrm{A}}$, which can be calculated from eqn. (2), and the area $(w_{\mathrm{m}}^2 - 1)\, r^2$ exposed to the atmosphere, which is calculated from eqn. (4e). X_{Zn} and X_{Cu} are the mass fractions of Zn and Cu of the bulk sample material, respectively. τ_{melt} is the time which is needed for solidification (*cf*. eqn. (6)). After insertion of the equations and some algebraic manipulation we yield

$$\frac{m_{\mathrm{Zn}}}{m_{\mathrm{Cu}}+m_{\mathrm{Zn}}}=\frac{X_{\mathrm{Zn}}\left[1+J_{\mathrm{Zn}}\tau_{\mathrm{melt}}r^2(w_{\mathrm{m}}^2-1)\frac{M_{\mathrm{Zn}}}{N_{\mathrm{A}}V}\right]}{X_{\mathrm{Cu}}+X_{\mathrm{Zn}}\left[1+J_{\mathrm{Zn}}\tau_{\mathrm{melt}}r^2(w_{\mathrm{m}}^2-1)\frac{M_{\mathrm{Cu}}}{N_{\mathrm{A}}V}\right]}$$

Fig. 7 a and b shows a fit of this model to values taken from the measurements of Cromwell and Arrowsmith[19] and Borisov *et al*.,[22] respectively. The applied fluence in this measurement was corrected due to the reflection. Only one fit parameter, the mean temperature of the melt at which evaporation takes place, was used. The fit temperature was found to be above melting and below the critical temperature of brass, which is reasonable because far away from the centre of the laser beam the temperature gradient is relatively insensitive to changes in the peak temperatures.[24] An excellent agreement between theory and experiment is found.

Some remarks need to be made. From the experimental side it is difficult to verify this model. Great care has to be taken to meet all requirements. Especially, if the ICP-signal is taken as a direct measure of "fractionation" one must keep in mind that the laser-evaporated material is not measured directly. The vaporized material is condensed, transported and again evaporated, atomized, ionized in the ICP, and only then it is detected. Using an ICP-signal requires that the aerosol is not dominated by large particles which are produced under the following conditions.

— Absorption is low and particles are removed by mechanical stress.

— Fluences are close to the ablation threshold. Here, no direct, congruent vaporization takes place and hydromechanical sputtering dominates.[46]

— Under atmospheres such as air, nitrogen, *etc*., which facilitate hydrodynamic sputtering.[47]

— Laser fluences are above the limit where plasma shielding occurs.

Therefore, if non-congruent evaporation effects are studied it is more conclusive to assess the primary aerosol directly. Up to now, this has only been done for a limited number of cases.[48–51] If experimental conditions are not carefully chosen, other effects, like incomplete evaporation in the secondary IC plasma, will overshadow the laser sampling effect. However, if it can be assumed that the laser generated aerosol consists mainly of small particles then the ICP signal is a good indicator for effects related to laser ablation. Thermodynamic or instrumental biases due the ionization are of minor interest on the scale that is used here. For instance, differences in ionization efficiency can be estimated on the basis of thermodynamic equilibrium. They yield 1.2 and 0.92 for Cu/Zn or Cu/Pb, respectively. Similar small factors can be expected for other instrumental biases.[52]

3.3. Optimal laser conditions

The model is based on several assumptions which describe the conditions that have to be met to achieve optimal, analytical laser sampling for the ICP. Explicitly, it is assumed that

- The liquid–vapour interface velocity in the vaporized volume is high enough to avoid fractionation
- Surface absorption takes place
- Stationary conditions are met
- Hydrodynamic sputtering is minimized.

In the following the first three assumptions will be discussed briefly, how they are achieved will be demonstrated, and what effects are occurring if they are not. The last assumption must be discussed in another framework. However, the implications are clear. If a thick, liquid melt layer exists, the prerequisite for melt displacement and hydrodynamic sputtering is met. With a reduction of the melt thickness (*i.e*., higher fluences) less and smaller particles are generated by hydrodynamic sputtering. Therefore, to employ the proposed model a certain fluence, which has to be determined later, must be applied. Otherwise fractionation will be under-estimated, because ICP effects related to incomplete evaporation of large particles are not

View Article Online

Published on 11 April 2006. Downloaded by Michigan State University on 19/01/2016 15:49:27.

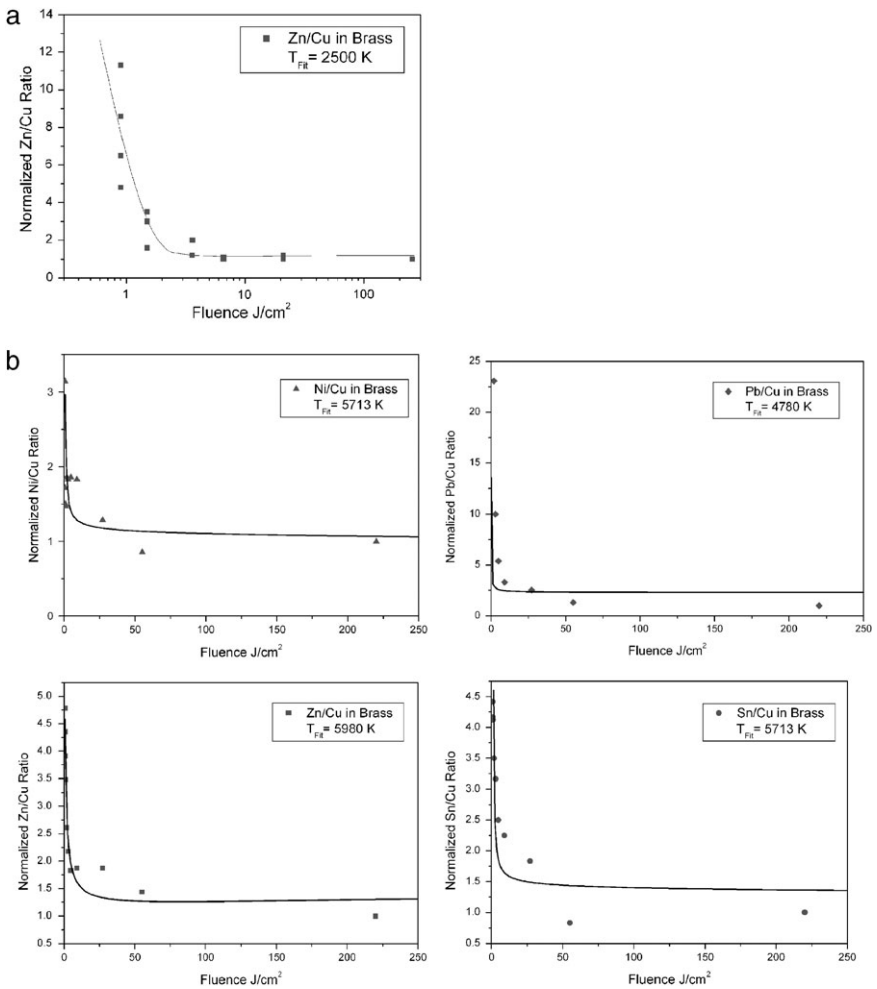

Fig. 7 (a) Comparison of literature data of a fluence dependent Cu/Zn ratio measurement taken from Borisov *et al.*,[20] with a calculation based on the proposed model. T_{Fit} represents the assumed melt temperature for the best fit. (b) Comparison of literature data of a fluence dependent element ratio measurement taken from Cromwell and Arrowsmith[17] with a calculation based on the proposed model. T_{Fit} represents the assumed melt temperature for the best fit.

included. Another way to meet the restrictions of the proposed model would be to remove larger particles generated due to a hydrodynamic mechanism by appropriate means.

3.3.1. Congruent vaporization. Up to now it has only been assumed that vaporization in the centre of the laser-produced crater is congruent. Fractionation appears at the outer, melted section. As already mentioned, according to the kinetic theory of gases, when a material evaporates into a gaseous medium the resultant evaporation rate near the interface is approximated by the Hertz–Langmuir–Knudsen equation, which together with the Clausius–Clapeyron relation defines the velocity of the evolving vapour–liquid interface (*cf.* eqn. (3)). Re-condensation of evaporated material on the sample surface is neglected.[9] These equations describe the evaporation of one component. If the liquid/vapour front evolves not too fast, a multi-component system can also be described by these equations. In such a situation the vapour is continuously removed from the surface. It is obvious that the composition of the vapour is different from the liquid in equilibrium with it. It will be in accordance with the appropriate liquid–vapour phase diagram. The less volatile species will be enriched in the melt until either the more volatile component is lost or a congruently evaporating (''azeotropic'') liquid mixture is reached.[53] Clearly, this situation is unfavourable for analytical purposes.

However, the described process depends on the presence of a diffusive maintained equilibrium in both the liquid and the vapour. Mass transport to the evaporating surface has to maintain the equilibrium. However, if the liquid/vapour interface is fast enough, only a surface layer of the liquid is depleted of the volatile species, the rate of the latter drops quickly and soon congruent vaporization is achieved. A qualitatively different situation may arise. If the melt consists mainly of a more volatile species, the less volatile will be dragged along. In the reversed case the more volatile is trapped by the less volatile species. However, the evaporation dynamics are described in both cases by the single component equation (*cf.* eqn. (3)). In the absence of a diffusive equilibrium the vapour composition approaches the composition of the liquid.

 This journal is © The Royal Society of Chemistry 2006

View Article Online

Published on 11 April 2006. Downloaded by Michigan State University on 19/01/2016 15:49:27.

Table 3 Calculated temperature, melt front velocity, and minimal laser fluence to achieve the critical velocity. The values in brackets indicate a possible variation of the surface temperature in the range of uncertainties of the thermodynamic data and the resulting variation of the depending variables

Element	T_{cr}/K	V_{cr}/cm s^{-1}	Min F_{cr}/J cm^{-2}
Cu	7290	2330	39
Fe	7880	2760	4
Al	4320 (3900)	2900 (2800)	110 (22)

The condition for this situation is that the evaporation interface velocity is faster than diffusive displacement, a condition that can be described as (see also eqn. (7))

$$v_{cr}(T) \geq \frac{D_L(T)}{4r}$$

D_L is the liquid phase diffusion coefficient of an alloying component in the liquid material, $4r$ a typical distance over which diffusion has to take place (*e.g.*, the radius of an atom). Due to the lack of reliable other data, temperature dependent, inter-metallic self-diffusion coefficients together with the liquid/vapour front velocity (*cf.* eqn. (3)) can be used, estimating the critical temperature, T_{cr}, and the velocity, v_{cr}, which has to be reached to ensure congruent vaporization.

From theory of corresponding states the diffusion coefficient can be estimated with appropriate accuracy.[54] We get

$$D_L(T) = f\left(\frac{T_{melt}}{T}\right)\sqrt{\frac{\varepsilon T_{melt} k_B N_A}{M}}\tilde{V}^{1/3}$$

Here, $f(T_{melt}/T)$ and ε (of the order 5.2) are empirically found parameters.[45,54] $\tilde{V}$ is the molar volume. It allows us to avoid any assumptions about the distance parameter if $r = \tilde{V}^{1/3}$ is assumed. Table 3 presents the results for 3 different metals, together with the fluence, calculated from eqn. (6), necessary to achieve the critical liquid/vapour front velocity. There are basically no data at hand which confirm these values. However, if these values are compared with Fig. 2, it seems feasible that the critical velocities for congruent, stoichiometric ablation are achievable. Also, Auger electron spectroscopic measurements of distributions of elements inside the crater indicate that congruent ablation is achieved in certain cases.[11] Critical fluences of approximately 10 J cm^{-2}, which mark the expected onset of congruent ablation, fit very well to known values for reduction of fractionation effects of Cu (brass) and steel samples.[19,21,22]

Al has been chosen to demonstrate a typical problem. Certainly, a calculated critical fluence of more than 100 J cm^{-2} is too high. However, already a variation of 10% of the surface temperature, which is in the range of uncertainty of thermodynamic constants of the material, decreases this value to 22 J cm^{-2}, whilst the critical velocity does not change much. It is very interesting to see that close analysis reveals that the surface temperature, T_S, is not the governing factor, it is the liquid/vapour front velocity ν_{cr} that has to be considered if congruent ablation is assessed.

3.3.2. Surface absorption. The second assumption is surface absorption. To have any effect on a material light must be absorbed. Although this primary interaction between light and matter is always non-thermal, it is often helpful to think of the absorption process as a secondary "source" of energy inside the material, which is driven by the incident beam but which tends to develop its own dynamic. It is the "secondary" source rather than the photons emitted by the laser which subsequently determines what happens to the irradiated material. This perception was explicitly used in the previous sections when thermal effects were calculated.

Explicitly, it was assumed that a thin, heated layer at the surface constitutes the secondary heat source and it was shown that optimal results can be achieved. Based on the previous results, the conditions that an ideal, "secondary" source for LA-ICP-MS purposes should meet, can be assessed and summarized as follows:

- high peak temperatures,
- maximum temperature at the surface,
- fast cooling and heating cycles (because stationary ablation was assumed),
- defined localization of the thermal energy.

As has already been discussed, "high" peak temperature has a clear, quantitative meaning related to the thermodynamic properties (*i.e.* diffusion coefficient, vapour pressure, *etc.*) of the material and guarantees congruent ablation. Again, it should be emphasized that, contrary to what is commonly is found in literature, it is possible to achieve congruent, stoichiometric ablation if the surface temperature is raised to a sufficiently high, but finite, temperature which ensures kinetic vaporization (*cf.* section 3.3.1). Under such circumstances the diffusive, maintained, thermodynamic equilibrium described by the Clausius–Clapeyron equation is disturbed and vaporization without changing the concentrations according to the vapour pressures of the different species at the surface takes place.

A temperature maximum at the surface (or close to the surface) is a requirement that is based on the trivial fact that evaporation takes place from the surface and efficient use of the delivered energy is only assured under these conditions. A second effect, sometimes encountered if maximum temperature at sub-surface occurs, is a mechanical disruption of top layers due to thermal stresses or explosive evaporation.[15] The mechanism results in large rupture fragments which are useless for analytical purposes.

Before a certain necessary temperature level is reached and before the material solidifies again, the material runs through temperature cycles, where detrimental effects (*e.g.*, fractionated evaporation) may occur. Therefore, minimizing these periods is advantageous.

Any de-localization of energy will increase the parasitic energy load in the non-ablated material. Different mechanisms such as, for instance, heat diffusion and mechanical displacement of the melt must be considered here, because all of them are clearly potential sources for a non-congruent sampling.

The question arises as to how these suppositions for an optimal "secondary" heat source can be achieved by controlling and optimizing the absorption process. To describe and discuss the absorption process we have to rely on some simplifications. Typically, the laser heated and ablated zone is small compared with the sample size and description as a semi-infinite substrate is appropriate. Additionally, a

View Article Online

Published on 11 April 2006. Downloaded by Michigan State University on 19/01/2016 15:49:27.

Gaussian beam profile is assumed as is that no phase transitions (*e.g.* melting) occur during the absorption process. This view is acceptable, because in the following the effect of depth distribution of laser energy on the resulting temperature distribution in an early time period is considered.

If we use Green's function technique to solve the heat conduction problem we yield (in dimensionless coordinates) for the temperature distribution inside the sample

$$\Delta\bar{T}(r=0,z=0,t)=\frac{2\tilde{\alpha}}{\sqrt{\pi}}\theta_{\mathrm{c}}\int_0^{t_{\mathrm{L}}}\frac{\mathrm{d}\tilde{t}}{1+4\tilde{t}}\mathrm{Erfc}(\tilde{\alpha}\sqrt{\tilde{t}})\exp(\tilde{\alpha}^2\tilde{t})$$

$$\tilde{t}=\frac{D_{\mathrm{th}}}{r_0^2}t,\tilde{\alpha}=\alpha r_0,\theta_{\mathrm{c}}=\frac{\sqrt{\pi}I_{\mathrm{A}}r_0}{2\kappa_{\mathrm{S}}} \qquad (8)$$

Here, α, I_{A}, D_{th}, and r_0 are the absorption coefficient, the absorbed fluence, the heat diffusion coefficient and the beam radius, respectively. If we look at the attainable peak temperature in the centre of the beam, we can characterize the influence of a finite absorption by normalizing the centre temperature of a substrate with finite absorption to the centre temperature of a substrate with infinite absorption. Then eqn. (8) gives

$$\Delta\bar{T}(r=0,z=0,t=\tau_{\mathrm{Laser}})=\frac{\Delta\bar{T}(0,0,t=\tau_{\mathrm{L}};\tilde{\alpha})}{\Delta\bar{T}(0,0,t=\tau_{\mathrm{L}};\tilde{\alpha}\rightarrow\infty)}.$$

As can be seen from Fig. 8 the centre peak temperature strongly increases with growing absorption. With (α r_0) > 100 surface absorption can be assumed. If we assume a laser spot of 50 μm this corresponds to an absorption coefficient $\alpha > 2 * 10^4$ cm^{-1}.

In contrast, similar considerations show that a variation of the absorption coefficient has only a little influence on the temperature distribution in the radial direction at distances larger than the absorption length.[24] Here, spatial beam shaping has much more impact on the confinement of the delivered laser energy.

To see how the duration of the heating period is influenced by absorption, the surface temperature growth has to be

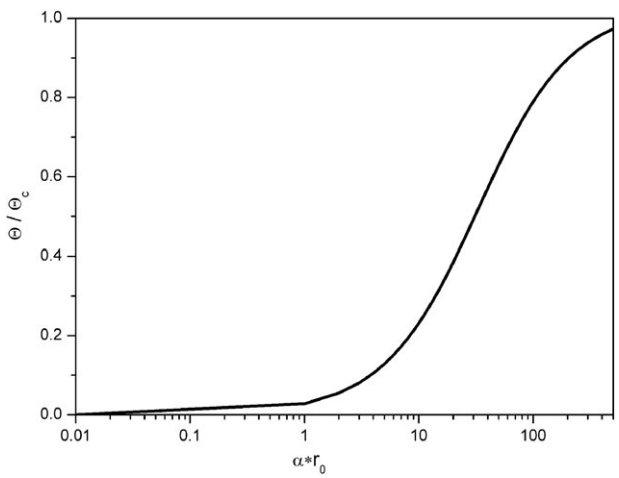

Fig. 8 Achievable centre temperature relative to infinite absorption as a function of the absorption coefficient.

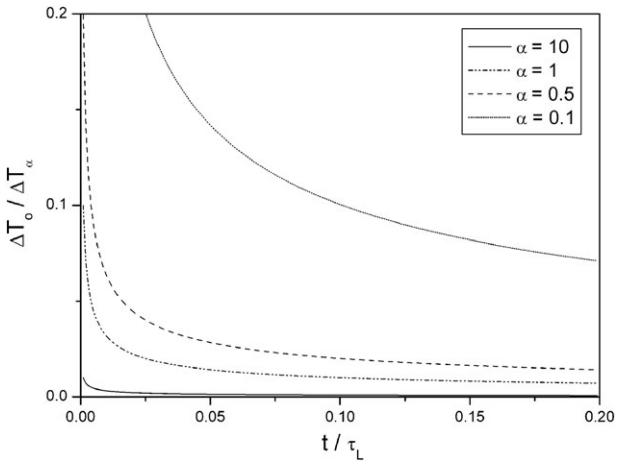

Fig. 9 With increasing absorption coefficient the time reduces that is necessary to achieve a temperature comparable with the infinite absorption case (ΔT_0). The time and temperature axes are normalized to laser pulse duration and maximum temperature, respectively.

estimated for early times during the laser pulse ($t < t_{\mathrm{laser}}$). In the cases of high absorption ($\alpha r_0 \rightarrow \infty$) and low absorption ($\alpha w_0 \approx 1$) the temporal temperature development can be estimated

$$\Delta\bar{T}(\tilde{\alpha}\rightarrow\infty)\approx\frac{4}{\pi}\theta_{\mathrm{C}}\sqrt{\tilde{t}}$$

and

$$\Delta\bar{T}(\tilde{\alpha}\approx 1)\approx\frac{2\tilde{\alpha}}{\sqrt{\pi}}\theta_{\mathrm{C}}\tilde{t}$$

respectively. Fig. 9 shows the trend: clearly the time to reach a satisfactory temperature at the surface is decreasing with increasing absorption.

A similar situation arises at the end of the laser pulse. At the onset of the cooling period directly after the laser pulse we can estimate the linear cooling rate as

$$\frac{\mathrm{d}\bar{T}}{\mathrm{d}\tilde{t}}\approx-\frac{\theta_{\mathrm{C}}\tau_{\mathrm{L}}}{3\sqrt{\pi}}\tilde{\alpha}^3$$

Thus, the cooling rate strongly increases with the absorption coefficient, $\tilde{\alpha}$. With increasing absorption the cooling period, and therefore the time where analytical negative effects occur, shortens. These results endorse the result of the 3-dimensional model calculations, where surface absorption was assumed.

Regardless off all further inspection, the results already show that a short optical penetration depth is a necessary condition to meet the previously mentioned analytical premises. If the absorption coefficient is larger than 10^4–10^5 cm^{-1} ($r_0 > 10$ μm), surface absorption is realized (*cf.* Fig. 8), which is, according to the given rationale, a necessary condition for optimal laser sampling for ICP-MS purposes.

However, it should be clearly seen that a sufficiently high absorption coefficient assures only that *if* enough energy is penetrating the sample, this energy is distributed in an optimal manner. What is enough energy for laser ablation without fractionation has to be estimated from the 3-dimensional model calculations.

 This journal is © The Royal Society of Chemistry 2006

View Article Online

Published on 11 April 2006. Downloaded by Michigan State University on 19/01/2016 15:49:27.

4. Conclusion

A model has been proposed that regardless of all necessary simplifications correlates systematic errors due to non-congruent evaporation and laser parameters such as laser fluence and wavelength, with material parameters such as, for instance, heat diffusivity and absorption in a realistic manner. For dilute alloys the model shows a good quantitative agreement with measurements taken from literature. Clearly, more experimental evidence is needed to justify and improve the calculations. However, the model has enough predictive power to allow several tests. Some future possible experiments that can be conducted are as follows.

- Energy dependent fractionation for more material systems.
- Crater size dependent fractionation effects.
- Measurement of melt thickness and melt depletion.

The model shows clear evidence that the fluence dependent fractionation effects can be related to surface temperatures not being high enough to reach the kinetic vaporization regime. On the other hand it is demonstrated that congruent vaporization is possible if a critical vapour/liquid interface velocity that depends on the surface temperature is transgressed. In that case, the melt removal is far from diffusive maintained evaporation equilibrium and the melt stoichiometry is not changed by the phase transition from liquid to vapour. To ensure optimal ablation conditions (*i.e.*, high surface temperature), it is necessary to match absorption and heat diffusivity with laser wavelength and pulse duration, respectively. Clearly, parameters like beam homogeneity are also influencing the fractionation. However, they are instrumental parameters that are not correlated directly with the material, and therefore easier to control.

In addition, it should not be overlooked that the model connects the internal problem with the external problem. Effects like hydrodynamic sputtering are dependent on a melt layer thickness. Further work will demonstrate the interdependence. From a practical point of view the model resolves theoretically the question of how optimal conditions in laser sampling for ICP-MS are achieved.

List of variables:

α	Absorption coefficient
α_g	Normalized plasma absorption coefficient
$\tilde{\alpha}$	Normalized, dimensionless absorption coefficient
α_0	Accommodation coefficient
c_P	Specific heat
D_{th}	Thermal diffusivity
D_L	Mass diffusion coefficient
F	Area
h	Plasma thickness
h_l	Melt thickness
ΔH_V^i	Vaporization enthalpy
ΔH_m	Melt enthalpy
I_A	Absorbed laser fluence
I_0	Laser fluence

(*continued*)

J, J_i, J_+, J_-	Particle fluxes
k_B	Boltzman constant
κ_S	Heat conduction coefficient
l_{th}	Thermal diffusion length
m_i, m^V, m^R	Mass
M_i, M	Molar mass
N_A	Avogadro constant
η	Radius of paraboloid curvature
ξ	
P_i	Partial pressure
P_S	Saturated vapour pressure
R	Reflectivity
r	Radius variable
r_0	Laser beam radius
R_V	Melt-to-vapour ratio
ρ, ρ_i	Liquid density
t	Time variable
T	Temperature variable
$\Delta\tilde{T}$	Dimensionless temperature variable
T_{melt}	Melting temperature
T_S	Surface temperature
T_0	Substrate temperature without laser heating
T_{cr}	Critical temperature (temperature corresponding to ν_{cr})
$\tilde{t}$	Dimensionless time variable
τ_L	Laser pulse duration
τ_{melt}	Melt solidification time
θ_c	Normalized, dimensionless centre surface temperature
V	Volume variable
$\tilde{V}$	Molar volume
v_{cr}	Critical velocity
v_{LV}	Liquid–vapour interface velocity
v_D	Heat diffusion front velocity
w, w_{melt}, w_{vapour}	Boundary parameter ($w_{vapour} = 1$)
X_{Zn}, X_{Cu}	Mass fraction
z	Depth variable

References

1 J. S. Becker and H. J. Dietze, *Int. J. Mass Spectrom.*, 2003, **228**, 127–150.
2 J. S. Becker, C. Pickhardt and H. J. Dietze, *Int. J. Mass Spectrom.*, 2000, **202**, 283–297.
3 L. Van Vaeck, H. Struyf, W. Van Roy and F. Adams, *Mass Spectrom. Rev.*, 1994, **13**, 189–208.
4 D. Günther, S. E. Jackson and H. P. Longerich, *Spectrochim. Acta, Part B*, 1999, **54**, 381–409.
5 K. Niemax, *Fresenius' J. Anal. Chem.*, 2001, **370**, 332–340.
6 D. Günther and B. Hattendorf, *Trends Anal. Chem.*, 2005, **24**, 255–265.
7 M. Tibi and K. G. Heumann, *J. Anal. At. Spectrom.*, 2003, **18**, 1076–1081.
8 C. A. Heinrich, T. Pettke, W. E. Halter, M. Aigner-Torres, A. Audetat, D. Günther, B. Hattendorf, D. Bleiner, M. Guillong and I. Horn, *Geochim. Cosmochim. Acta*, 2003, **67**, 3473–3497.
9 S. I. Anisimov, Y. A. Imas, G. S. Romanov and Y. V. Khodyko, *Action of high-power radiation on metals*, Consult. Bureau, Springfield, VA, 1971.

View Article Online

Published on 11 April 2006. Downloaded by Michigan State University on 19/01/2016 15:49:27.

10 R. E. Russo, X. L. Mao and S. S. Mao, *Anal. Chem.*, 2002, **74**, 70 A–77 A.
11 R. Hergenröder, M. Samoc and V. Hommes, *Mass Spectrom. Rev.*, 2006, published online DOI: 10.1002/mas.20077.
12 R. Hergenröder, *Spectrochim. Acta, Part B*, 2006, in the press.
13 G. Callies, P. Berger and H. Hugel, *J. Phys. D: Appl. Phys.*, 1995, **28**, 794–806.
14 X. L. Mao, W.-T. Chan, M. Caetano, M. A. Shannon and R. E. Russo, *Appl. Surf. Sci.*, 1996, **96–98**, 126–130.
15 R. L. Webb, J. T. Dickinson and G. J. Exarhos, *Appl. Spectrosc.*, 1997, **51**, 707–717.
16 J. Koch, I. Feldmann, B. Hattendorf, D. Günther, U. Engel, N. Jakubowski, M. Bolshov, K. Niemax and R. Hergenröder, *Spectrochim. Acta, Part B*, 2002, **57**, 1057–1070.
17 A. Bogaerts, Z. Chen, R. Gijbels and A. Vertes, *Spectrochim. Acta, Part B*, 2003, **58**, 1867–1893.
18 L. Wang, I. S. Borthwick, R. Jennings, P. T. McCombes, K. W. D. Ledingham, R. P. Singhal and C. J. McLean, *Appl. Phys. B: Photophys. Laser Chem.*, 1991, **53**, 34–38.
19 E. F. Cromwell and P. Arrowsmith, *Appl. Spectrosc.*, 1995, **49**, 1652–1660.
20 E. F. Cromwell and P. Arrowsmith, *Anal. Chem.*, 1995, **67**, 131–138.
21 M. Gagean and J. M. Mermet, *Spectrochim. Acta, Part B*, 1998, **53**, 581–591.
22 O. V. Borisov, X. L. Mao, A. Fernandez, M. Caetano and R. E. Russo, *Spectrochim. Acta, Part B*, 1999, **54**, 1351–1365.
23 S. F. Durrant, *J. Anal. At. Spectrom.*, 1999, **14**, 1385–1403.
24 D. Bäuerle, *Laser Processing and Chemistry*, Springer-Verlag, Berlin, 3rd edn., 2000.
25 X. L. Mao, W. T. Chan, M. A. Shannon and R. E. Russo, *J. Appl. Phys.*, 1993, **74**.
26 S. S. Mao, X. Mao, R. Greif and R. E. Russo, *Appl. Phys. Lett.*, 2000, **77**, 2464–2466.
27 C. Liu, X. Mao, S. S. Mao, R. Greif and R. E. Russo, *Anal. Chem.*, 2005, **77**, 6687–6691.
28 F. Poitrasson, X. L. Mao, S. S. Mao, R. Freydier and R. E. Russo, *Anal. Chem.*, 2003, **75**, 6184–6190.
29 V. Margetic, A. Pakulev, A. Stockhaus, M. Bolshov, K. Niemax and R. Hergenröder, *Spectrochim. Acta, Part B*, 2000, **55**, 1771–1785.
30 O. Samek, V. Margetic and R. Hergenröder, *Anal. Bioanal. Chem.*, 2005, **381**, 54–56.
31 S. I. Anisimov and B. S. Luk'yanchuk, *Physics-Uspekhi*, 2002, **45**, 293–324.
32 H. S. Carslaw and J. C. Jaeger, *Conduction of Heat in Solids*, Clarendon Press, Oxford, 1988.
33 A. Egbert, B. Mader, B. Tkachenko, C. Fallnich, B. N. Chichkov, H. Stiel and P. V. Nickles, *Appl. Phys. Lett.*, 2002, **81**, 2328–2330.
34 J. P. Hirth and G. M. Pound, *Condensation and Evaporation*, Pergamon Press, Oxford, 1963.
35 Y. I. Frenkel, *Kinetic Theory of Liquids*, Oxford University Press, Oxford, 1975.
36 E. N. Sobol, *Phase Transformations and Ablation in Laser-Treated Solids*, John Wiley & Sons, 1995.
37 M. M. Martynyuk, *Russ. J. Phys. Chem.*, 1979, **53**, 1080–1081.
38 A. Bogaerts and Z. Chen, *Spectrochim. Acta, Part B*, 2005, **60**, 1280–1307.
39 H. Schmidt, J. Ihlemann, B. Wolff-Rottke, K. Luther and J. Troe, *J. Appl. Phys.*, 1998, **83**, 5458–5468.
40 N. Arnold, J. Gruber and J. Heitz, *Appl. Phys. A*, 1999, **69**, S87–S93.
41 S. Eliezer, *The interaction of high-power lasers with plasmas*, Institute of Physics Publishing Ltd., 2002.
42 C. L. Chan and J. Mazumder, *J. Appl. Phys.*, 1987, **62**, 4579–4586.
43 C. Chaléard, P. Mauchie, N. Andre, J. Uebbing, J. L. Lacour and C. Geertsen, *J. Anal. At. Spectrom.*, 1997, **12**, 183–188.
44 S. Laville, F. Vidal, T. W. Johnston, O. Barthe'lemy, M. Chaker, B. Le Drogoff, J. Margot and M. Sabsabi, *Phys. Rev. E*, 2002, **66**, 0066415.
45 T. Iida and R. I. Guthrie, *The physical properties of liquid metals*, Clarendon Press, Oxford, 1988.
46 R. Kelly and J. E. Rothenberg, *Nucl. Instrum. Methods Phys. Res., Sect. B*, 1985, **7–8**, 755–763.
47 R. Hergenröder, *J. Anal. At. Spectrom.*, DOI: 10:1039/b600705h.
48 P. Weis, H. Beck and D. Günther, *Anal. Bioanal. Chem.*, 2005, **381**, 212–224.
49 R. Jaworski, E. Hoffmann and H. Stephanowitz, *Int. J. Mass Spectrom.*, 2002, **219**, 373–379.
50 J. Koch, A. von Bohlen, R. Hergenröder and K. Niemax, *J. Anal. At. Spectrom.*, 2004, **19**, 267–272.
51 H. R. Kuhn, M. Guillong and D. Günther, *Anal. Bioanal. Chem.*, 2004, **378**, 1069–1074.
52 A. Montaser, *Inductively Coupled Plasma Mass Spectrometry*, Wiley–VCH, Inc., New York, 1998.
53 M. von Allmen and A. Blatter, *Laser beam interactions with material*, Springer Verlag, Berlin, 1998.
54 A. D. Pasternak, *Phys. Chem. Liq.*, 1972, **3**, 41–53.

 This journal is © The Royal Society of Chemistry 2006